Nanoparticle-reinforced AA6061-T6 friction stir welded joints: mechanical and microstructural characteristics

Jagannath Mohapatra
College of Engineering Bhubaneswar, Biju Patnaik University of Technology, Odisha

A B S T R A C T

This study examines how the distribution of nanoparticles affects the mechanical and metallurgical properties of FSW welds in relation to the reinforcement technique. Additionally, optical microscopy (OM), scanning electron microscopy (SEM), and transmission electron microscopy (TEM) were used to analyze the size and dispersion of reinforcement particles in different zones of the FSW process. More attention was paid to the processed zone (nugget zone) while evaluating the micro-hardness of the unreinforced and reinforced samples. This zone is further associated with the size and shape of the particles. The results showed that, in comparison to the FSW-TiO2 sample, the refinement of grain size is more significant in the nugget zone of the FSW-Al2O3 sample. This is explained by the Zener-effect, which is caused by small-sized nanoparticles and helps to limit the growth of grains along with dynamic recrystallization during the FSW process. When compared to the parent metal, the processed zone's micro-hardness increased due to a uniform distribution of Al2O3 nanoparticles, reaching a peak micro-hardness of 89 ± 3 HV. However, surface defects resulted from a decrease in the distribution of TiO2 nanoparticles, which increased grain size and decreased material strength, with an average micro-hardness of 78 ± 5 HV. The mechanical results showed that the presence of TiO2 nanoparticles causes a decrease in tensile properties due to nanoparticle cluster formation, which in turn causes a decrease in ductility, wear resistance, and an increase in frictional coefficient. In contrast, the high density of uniform Al2O3 nanoparticle distribution in the nugget zone results in an increase in tensile strength, yield strength, and wear resistance with a noticeable increment in ductility.

Keywords: AA6061-T6, Friction stir welding Reinforcement particles Microhardness distribution Mechanical characteristics Wear characteristics

1. Introduction

In order to meet the demands of modern technical applications, product design optimization for lighter materials is now required by the aerospace, automotive, and marine industries [1]. To that end, the industry offers a wide variety of engineering light materials, such as alloys made of magnesium, titanium, and aluminum. Aluminum is utilized in the shipbuilding, transportation, aircraft, and marine industries, among other areas, due to its strong corrosion resistance and strength to weight ratio [1-3]. The most appropriate alloy for marine frames, pipelines, airplanes, and other applications is thought to be the heat-treatable 6xxx (Al-Mg-Si) series alloy, which includes AA6061 [4,5]. In order to attain high creep resistance at extreme temperatures, reduced activation ferritic/martensitic steels (RAFM) [6] and austenitic steel [7] with a high percentage of chromium content have found extensive use in the fossil fuel and nuclear power industries in recent years. Conventional fusion welding techniques are known to present challenges when joining aluminum alloys and these steels. These techniques may result in a number of obstacles, including low weldability, solidification cracking, distraction stress, and the formation of many more brittle intermetallic phases (for aluminum alloys) [10], as well as an acceleration of joint creep damage at high temperatures, lower creep strength, shorter rupture times than that of the base material, and fumes of hexavalent chromium (for steels) [11]. These issues may arise during the inevitable process of joining the materials. Furthermore, reduced creep strength and a shorter carbide dissolving time in austenitic and RAFM steels, as well as poor wear resistance and erosion in aluminum alloys, are significant concerns for prolonged utilization [5, 7]. The creep properties of RFAM steel weldment are negatively impacted by the heterogeneous microstructure of the heat affect zone (HAZ), which is a major in-service issue [6,11]. In contrast, for precipitation strengthening aluminum alloy, the processed weld area always has lower properties than the base material, particularly mechanical properties, and is likely to fail from the nugget zone. More intricate factors, such as the uneven

dispersion of ceramic particles, the coarsening and dissolution of precipitates, particularly in the welded zone area, etc., contribute to the weakening of this zone [4,5]. Given these restrictions, the design and joining problems would be resolved by using a technique for joining aluminum alloys and steels that is controlled by the melting point of the specific workpiece material [10,12]. Friction stir welding (FSW) is a more effective method of resolving these kinds of problems since it does away with the imperfections that arise from fusion welding steel and aluminum alloys. In order to meet high ratios of strength to weight, high corrosive resistance, and high temperature service conditions in the automotive, marine, and nuclear power industries, friction stir welding (FSW), a solid-state welding process, has become more and more appealing in recent years for fabricating and joining weld structures on various base metal-matrix, including aluminum, titanium, ferritic/martensitic/austenitic steel, copper, magnesium, and metal-matrix composites [6,7,10,13–16]. Moreover, the recent improvement in FSW tool materials, such as WeRe alloy and polycrystalline cubic boron nitride (PCBN), have en- large the field of applications for welding steels [7,11]. FSW process also helps to retain the original distribution of ceramic particles in the welded area which leads to enhancement in property gradient [3,15]. Previous works reported that the FSW weldability of reduced activation ferritic/martensitic steels is good and revealed the potentiality for achieving high quality welds [7,14]. The microstructures and proper- ties of FSW joints on RAFM steels may show much difference compared with that of fusion welding technologies due to the special FSW process, which is based on frictional heating, plastic flow and plastic deforma- tion of the materials in weld regions [6,11,14]. FSW is patented and proven via experiments at The Welding Institute (TWI) in the UK in December 1991 is a viable process in which rotating tool once it tou- ches the workpiece surface via plunging and move along the joint in- terface of adjoining surface, the material gets soft due to the local heat intensity formed during stirring action of tool, that leads to more re- circulation of plastically deformed material near the tool surface that encourages deformation (plastic) and leads to joining in solid-state [4,6]. Recently, to evaluate the viability of FSW in order to join various alloys, steels, and reinforced Al-matrix composites using various re-inforcement particles, several studies have been conducted, e.g., copper [15], ferritic/martensitic/austenitic steel [6,7,11,14], magnesium [16], titanium [13] and various MMCs

including 7005/Al_2O_3/10p [17], 6061/TiC/(3p & 7p) [18], 2124/SiC/25p [19] and others [20–22]. are successfully welded via FSW. Recently, Friction stir processing (FSP) alternative to the FSW process was evolved for microstructural features modifications of various metals and alloys. The initial work was in- itiated by Mishra et al. [4] to produce composite via FSP by placing the reinforcement particles in the form of a slurry (pre-mixed with volatile solvent) as a coating layer on the upper surface of AA5083 alloy. They found appreciable enhancement in the properties in terms of mechan- ical strength and microhardness (175 HV) was achieved which is almost double to that of the base material (85 HV). This work opens the numerous ways and possibilities to accomplish the uniform reinforcement particles (RPs) dispersion in metallic-matrix. Further, attempts were devoted to producing bulk metal matrix composites (MMCs) via dif- ferent particle pre-deposition methods via FSP [23–26]. Advancement in these modern procedures was done to abolish unwanted operations and to avoid the loss of (RPs) that would spread out during the process. Several studies were conducted in the past based on successful fabri- cation of different MMCs via FSP by employing various deposition strategies, like, drilled holes method [23,24], groove method [25,26], direct pasting [4,27] to evaluate the influence of rotating tool speed, transverse speed, number and direction of FSP passes, etc. on properties of produced composites. However, the influence and the role of the addition of nanoparticles on morphology and distribution of RPs in terms of precipitates in different zones of AA6061-T6-FSW joints were not discussed so far. The deposition method is important for con- sistency, homogeneity, and spreadability of embedded RPs that could affect the material attributes based on the property gradient [28–30]. Defect-free and uniform dispersion of RPs in single FSWFSP pass is a demanding problem that leads to an asymmetric flow of material [25–27,31,32] that nowadays can be reduced via, multi-pass, shifting of tool rotation during the process, etc. But such methods have limitations as RPs either would spread out or accumulate in the burrs while increasing the number of passes due to which only a small fraction of RPs was immersed inside the base material that leads to increase the cost and time requirements for the process to complete [33–35]. In respect to these limitations, the evolution of procedure that helps in reducing the ejection of RPs from joint interface and improvement in uniformity of RPs within the given cost and time to go long way for joining of aluminium alloy via single FSW pass. An

effort is made in this direction by incorporating the new deposition strategy in which slurry of RPs was employed to embed in Zig-zag holes (cylindrical) drilled in an array form on adjoining faces of 6061-T6 aluminium alloy sheets. The foremost advantages of the suggested approach of employing na- noparticles slurry are, (1) the concentration of nano-sized particles was increased for any specific reservoir volume, which is attributed to the fact that dry powders have always low density, (2) the percentages of soaring particles in the air were significantly reduced during pre-de-position and FSW, (3) RPs would keep inside in the vicinity between edges during the FSW process by providing good interfacial bonding and vigorous inter-mixing, that leads to increase in property gradient. This suggested novel proposal has never been tried or applied by re- searchers in the past according to the International literature available for different metal-based alloys. This step will open an entirely new outlook towards better utilization and distribution of RPs in the metal matrix by eliminating the problem of scattering and loss of RPs within the Al-matrix. Sun et al. [35] have used SiC as reinforcement particles which are embedded in the gap of 1 mm in the faying edges of Cu-plates and successful in producing Cu-composite in the weld zone via FSW. Bahrami et al. [32] have found promising results by employing the FSW process to join AA7075 by incorporating SiC reinforcement particles along the joint line. They observed the excellent bonding occurred between the substrate/RPs interfaces and obtained the pragmatic in- fluence of SiC particles on the absorption of impact energy. More re-cently, Saeidi et al. [17] had applied FSW to evaluate the effect of Al_2O_3 nanoparticles (by placing on joint interface), on mechanical, corrosion, and toughness behaviour of AA5083/AA7075 + Al_2O_3 dissimilar joint and found that with the addition of Al_2O_3 nanoparticles the toughness as well corrosion resistance of joint was improved compared with un-reinforced alloy. From the literature, it was found that most of the existing research work published uses an impromptu RPs deposition method to evaluate the consequence of RPs, processing specifications, and geometries of the tool on the surface, physio-mechanical and cor- rosion properties of FSW joints. However, the effect of size and dis- tribution of RPs in various zones of FSW for AA6061-T6 joints and their mechanism along with the reason for increment in mechanical prop-

erties is not discussed so far to the best of knowledge of the author. In the present work, FSW of AA6061-T6 joints were done based on the novel proposed

reinforcement deposition strategy. Also, the present work focussed on to study the influence of aluminium oxide (Al2O3) and titanium oxide (TiO2) nanoparticles distribution in various FSW zones on macro-microstructural characterization, grains structure evolution, mechanical behaviour, microhardness, and tribological aspects, to en- hance the RPs distribution for increment in property gradient.

Materials and methods

Thin sheets of AA6061-T6 with dimension (200 × 100 × 2.5) mm3 and chemical composition (wt%) Mg (0.901), Si (0.615), Fe (0.304), Cu (0.258), Mn (0.0454), Cr (0.19), Ni (0.013), Zn (0.054), Ti (0.0195), Pb (0.0030) and Sn (< 0.01000) were taken as parent material. Nano Partech Chandigarh supplied Al2O3 and TiO2 nanoparticles with 99.99% and 99% purity with a specific surface area of > 30. SEM was used to assess the average grain size of Al2O3 nanoparticles (15 nm) and TiO2 nanoparticles (15 nm). It is important to consider both the structure/morphology of nanoparticles and their impact on the dis- persion in the welded area. Both nanoparticles used in this study have the same structure and size with spherically shaped balls of the irre- gular pattern as shown in Fig. 1a, b. In this study, FSW was conducted
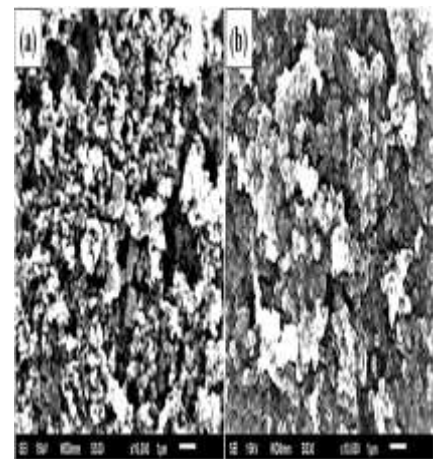

Fig. 1. SEM micrographs: (a) Al_2O_3 Nanoparticle, (b) TiO_2 Nanoparticle., Note: SEM: Scanning Electron Microscopy, Al_2O_3: Aluminium oxide, TiO_2: Titanium oxide.

by incorporating reinforcement particles (in slurry form) into 30 holes (cylindrical), (15 holes per sheet) with 1.5 mm of diameter and depth 3 mm was drilled at the adjoining edges of AA6061-T6 sheets as shown in Fig. 2a. The entire procedure of reinforcing nanoparticles in the base aluminium matrix was mentioned in the previous research [36]. Ac- cordingly, the calculated density of dried slurry for Al2O3 nanoparticles and TiO2 nanoparticles was found to be

2.362 g/cm3 and 3.627 g/cm3, respectively. Theoretical reinforcement particle volume percentage in drilled holes was estimated as 3% for both the nanoparticles. FSW of reinforced 6061-T6 aluminium alloy sheets was conducted on a dedi- cated machine for FSW (VMC-TC-1200) their schematic and modified fixtures designed for experimentation are shown in Fig. 2b, c. FSW tool was fabricated using H13 steel having a pin (cylindrical) of the round base (used to increase the tool life with less material wear) of diameter 5 mm and length 2.30 mm and concave shoulder of 3° concavity with 15 mm diameter was utilized and their schematic is shown in Fig. 2d. FSW tool was positioned at a central joint line of the sample before FSW was conducted. Based on the previous research [36], optimum process parameters such as 2000 rpm of tool rotating speed, 70 mm/min of transverse speed, 0° tilt of tool (used to ensure the proper contact be- tween the tool shoulder and the workpiece, to facilitate the flow of the material around the tool, and to avoid the thinning of the sheets from the nugget zone which lead to defective weld), 15-sec dwell, and

0.2 mm depth of plunge were selected for friction stir welding of

AA6061-T6 unreinforced and reinforced samples. Samples without nanoparticle addition were used for comparison purposes with re- inforced samples to evaluate the influence of nanoparticle dispersion on flow behaviour in terms of mechanical action. For macro and micro- structural studies, the 10 mm × 10 mm cross-section of the specimen was cut from the nugget zone of both unreinforced and reinforced friction stir welded samples as shown in Fig. 2e. Afterward, the samples for metallurgical examinations were prepared using different SiC abrasive grit quality papers followed by mechanical polishing up to

0.25 μm diamond suspension and etching using Keller's solution.

Thereafter, microstructural features of base material, with and without nanoparticles based samples were obtained and analysed using OM (Leica DM 2700 M), SEM (Jeol-124Nx, Japan) and TEM (Jeol-432 TXC, Germany) and grain size in different zones of FSWed samples (with and without nanoparticles addition) was calculated using Image analysis software according to ASTM-E112 intercept method. Vickers micro- hardness tests were done according to ASTM-E384 on samples at 1 mm distance below the top surface on distinct points from both sides of the nugget zone. The load was set at 200 g and exerted on the sample for 15 s. ASTM-E8M-11 was used to cut three samples each from one set of FSWed sheets for calculating the average of three

values for tensile properties. For tensile testing, a cross-head speed of 2 mm·min−1 was

used and tests were performed in ambient condition on the universal testing machine (UTE 80-3/92-1505). Wear tests were performed on the top surface of weldments using a normal load of 15 N and rotational (rpm) and sliding velocities (mm/s) of 142 and 0.07using the pin-on- disk machine.

Results and discussion

Characterization and microstructural features of AA6061-T6

Fig. 3a, b depicts the microstructural representation for AA6061-T6 (as the base material) in the horizontal and vertical direction and it has been found that both sections were identical with the ASTM grain size of (G ~ 35–38 μm). From Fig. 3, it was observed that the grains of parent metal were more elongated in nature towards the direction of

rolling due to the manufacturing process [29,37]. Also, it was observed that numerous forms of second phase particles were also present those are distributed uniformly in the Al-matrix and orient more towards the rolling direction. Fig. 4 presents the morphology of primarily three different forms of intermetallic second phase particles found in the AA6061-T6 base material before FSW. From Fig. 4a, it can be observed

that most of the Mg_2Si phases were dissolved in the α-Al matrix that is evenly dispersed in the base material and only a few rectangular-shaped

particles were available that provides the oxygen in large percentage on the surface of the AA6061-T6 sheets [38]. Also, few Al5FeSi particles were present in different shapes and sizes with angular and spherical morphology as shown in Fig. 4b. Therefore, due to the presence of these particles in large size with brittle nature, it makes difficult for dis-

solution in the α-Al matrix. But, because of the plastic deformation

occurred during FSW it leads to breaking up and settled down of these particles with uniform dispersion in the Al-matrix [12,39]. Fig. 4c shows the Al12(Fe Mn)3 Si or Al12(Fe Cr)3Si particles with similar morphology as intermetallic compounds of Al-Fe-Si.

Macro and microstructural features of AA6061-T6 with TiO2 nanoparticles

Macroscopic features
Friction stir welded samples with TiO2 nanoparticles

were visually inspected at the macroscale level for outward imperfections and flow behaviour due to the action of local stress and welding parameters. Fig. 5 shows the macro and microstructural features of AA6061-T6/ TiO2 friction stir welded samples. Fig. 5a depicts the geomorphological of weldment which has a rough appearance with cavity like a defect near the end of the joint. Fig. 5b depicts the macrographs for the FSW- TiO2 sample that does not show proper consolidation of deformed
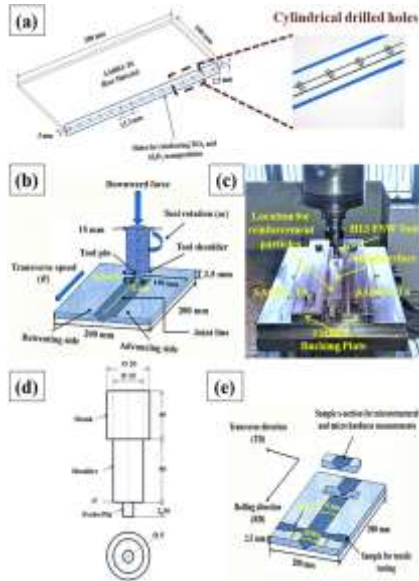

Fig. 2. Layout of the experimental study (a) Method of nanoparticles embedment in the Al-matrix, (b) Schematic of the FSW process, (c) Scheme of fixture for the FSW process, (d) Dimensions of FSW tool (e) Depicting how samples were extracted for various characterization tests.

material and found some nanoparticles accumulation beneath the HAZ towards the AS. This was attributed to the reason that, at the trailing edge of advancing side, due to lower momentum occurred between the tool and transported/deformed material, the flow of the plasticized material is less intense [30,40], whereas, the increment in localized heat due to high rotational speed results in good homogenization of nanoparticles in the weld nugget zone with more expansion on RS [41]. The reason for this expansion is the higher temperature and lower

relative particle velocity on AS compared to RS, because of which with the forward transverse of the rotating tool the deformed forged softer material in RS is more extruded and dispersed about AS. These results are in better agreement with the previous studies [6,27,33,42]. Mac- rographs (Fig. 5b) also indicates that the vortex shape nugget zone was generated with nanoparticles accumulation on AS because metal-flow movement about the rotating pin is strongly influenced

by mainly two components of dynamic flow, (a) rotational speed, (b) vortex ring
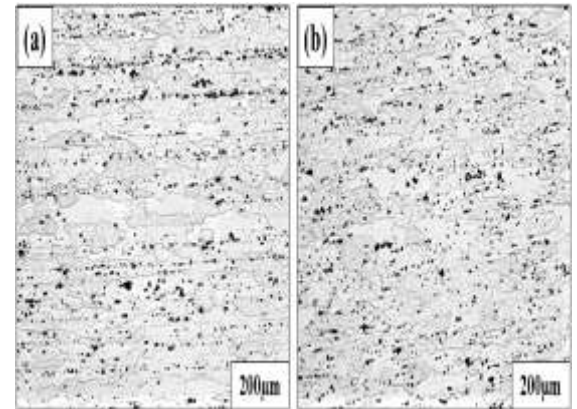

Fig. 3. Micrographs of AA6061-T6 parent material: (a) Horizontal direction, (b) Vertical direction.

circulation which is occurred via tool stir action and transverse motion of plasticized material along the welding direction [31,36].

In-depth TiO2 nanoparticles distribution

For in-depth TiO2 nanoparticle distribution in various FSW zones, a cross-section of friction stir welded samples were cut in the transverse direction to reveal the microstructural features of the processed zone (nugget zone) in terms of size and distribution using material char- acterization techniques. It was observed that the great amount of TiO2 nanoparticles would be immersed within the Al-matrix when single FSW pass at higher rotating (2000 rpm) and lower travel (70 mm/min) speed opted with some nanoparticles accumulation on AS which is due to lower particle velocity. But as the number of runs increases, it results in a small fraction of nanoparticles would be submerged in the matrix because the nanoparticles would either dissipate (lost) or settled down

in burrs after every run due to the effective stirring of the tool during FSW process [25,39]. Distribution and size of TiO2 nanoparticles in the various zone of FSWed-AA6061-T6 joints were explained by using op- tical micrographs as illustrated in Fig. 5. According to Fig. 5, base

material mainly composed of more elongated grains with average particle size of about 38 μm, while, heat-affected zone (HAZ) (Fig. 5c) influenced by thermal cycle only and does not induce plastic de- formation results in agglomeration of TiO2 nanoparticles (Region A)

along the AS which is attributed to insufficient heat input that leads to strengthening precipitates becomes

coarser and increase in precipita- tion free zone [43]. The mechanism behind this is that the solute pre- cipitates which are gathered in the form of clusters would impede the movement of dislocation under stress, which results in increment in material strength due to the interaction of precipitates with dislocation at the interface [28,40]. Fig. 5d depicts the generation of fine
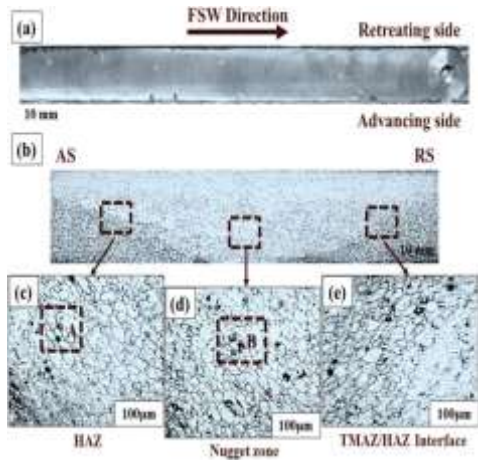

Fig. 4. SEM images of morphology of intermetallic compounds found in the 6061-T6 aluminium alloy: (a) Mg_2Si-phase; (b) Al_5FeSi phase; (c) $Al_{12}(FeMn)_3Si$ phase.

Fig. 5. Macro and micrographs of AA6061-T6- TiO_2 processed FSWed sample, (a) Typical surface morphology of sample with TiO_2 nanoparticles, (b) Cross-sectional macrographs of FSW-TiO_2 weldment, (c) HAZ on AS with TiO_2 nanoparticles agglomeration and sub-grain boundaries (Region A), (d) NZ with fine grains morphology with few agglomerated particles (Region B). (e) TMAZ/HAZ interface on RS: Note- FSWed:- Friction stir welded, HAZ:-Heat affected zone, NZ:-Nugget zone, TMAZ:- Thermo-mechanical affected zone, RS:-Retreating side, AS -Advancing side.

dynamically recrystallized grains microstructure in the nugget which is more attributed to plastic deformation (severe) and friction heating occurred during FSW via a phenomenon known as dynamic re- crystallization. This phenomenon was distinguished by coalescence and rotation of sub-grain via grain growth and nucleation which leads to the generation of high angle grain boundaries [44]. Because of TiO2 na- noparticle presence, the processed zone has a granularity of 8 µm which is more associated with Zener-effect which retards the granular growth

in the aluminium metal-matrix. Due to this phenomenon, the addition of nanoparticles influenced the fine particles dispersion by providing the Zener- pinning force on high and low angle grain boundaries movement to prevent their motion and opposes the force (driven) ap- plied on these grains interfaces (boundaries) [24,42]. In this study, the limiting grain size was evaluated using Zener relationship,(DZ = 4r/ 3Vf), such as r and Vf represents the radii and cross- sectional volume reinforcement fraction for sample reinforced with TiO2 nanoparticle

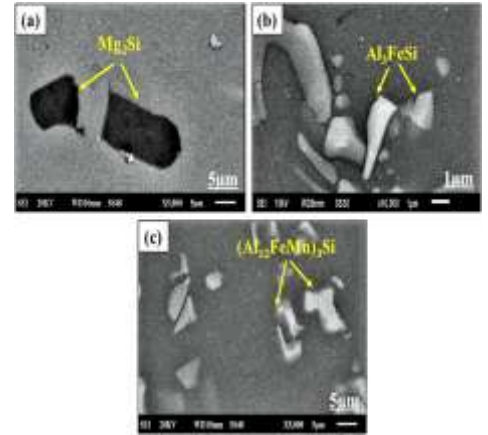and the calculated DZ was 8.2 µm which is more similar

when compared

to DZ based on the linear intercept method. Fig. 5e shows a distinct boundary of TMAZ and HAZ on RS where it experienced less strain and strain rates with lower peak temperatures. As a result, elongated grains present at the adjoining of nugget zone and parent metal (38 µm) governs the shearing action of metal- flow about the tool rotation.

Therefore, the material is deformed plastically by stirring action of tool pin and heat-affected this zone which is not sufficient for re- crystallization (dynamic) to occur, due to this size of grains in the TMAZ is bit large (15 µm) than nugget zone. These results are in better agreement with the findings of Zhang et al. [6]. Fig. 6 shows the

transverse section of TiO2 nanoparticle reinforced AA6061-T6 samples fabricated via FSW. Fig. 6a shows the non-uniform distribution of TiO2 nanoparticles with agglomeration on AS towards the HAZ. The most important reasons for the agglomeration of TiO2 nanoparticles in AS than RS are (a) less heat and partial fragmentation occurs in this zone,

lower thermal cycle in RS due to opposite tool rotation and more enhanced fluidity and displacement of material in the AS due to the parallel direction of tool rotation in respect to the transverse direction,

due to TiO2 nanoparticles dispersion in parallel bands and stretched along the direction of shear stress in the Al-matrix. With the addition of TiO2 nanoparticle, there is a considerable reduction in the granular size of nugget compared with a base material that is ascribed to the pinning of grain boundaries of second phase particles and reinforcement par- ticles [28,45]. Fig. 6b shows the SEM micrographs of HAZ (highlighted Region A) which represents TiO2 nanoparticle agglomeration on ad- vancing side with few primary (Al-Fe-Mn-Si, Mg2Si) and secondary (Al- Fe-Mn-Si-Cr) particles with complex precipitates structure which

results in coarsening of nanoparticles that leads to increment in micro-hard- ness. This was attributed to the fact that, the inter-metallic and TiO2 nanoparticles would undergone fracture process and partial fragmen- tation, as a consequence of low localized heat input and stirring caused by the pin, whereas, Fig. 6c depicts the SEM micrographs of nugget zone (Region B) which represents the non-uniform dispersion of TiO2 nanoparticles due to decreased volume fraction tendency of Al12(Fe Mn)3Si and Mg2Si. Further, the reduction of Al12(Fe Mn)3Si phases in the nugget zone was due to breaking, re-distribution and severe plastic deformation process [40,43] occurred during the FSW process, as si- milar findings were obtained by Fernandez et al. [25]. Fig. 7 shows the high-resolution TEM micrographs of FSW-TiO2 welds depicting the clear understanding of grain structure and precipitates. Fig. 7a,b depicts the coarse grain structure with elongated grains (Fe, Mn, Cr)3SiAl12 particles and round Mg2Si precipitates with some unreacted TiO2 na- noparticles that are formed at the Al/TiO2 interface. This was attributed to the SPD process and reactions via diffusion (solid-state) that occurred during the FSW process, because of which many Al2O3 nanoparticles would nucleate and grow at the Al/TiO2 interface [28,46]. When the reaction between the Al-TiO2 particles precede further, the excessive

SEM micrograph of HAZ on AS (Region A) depicts the formation of primary and secondary particles along with TiO$_2$ nanoparticle agglomeration, (c) SEM micrograph of NZ (Region B) show non-uniform TiO$_2$ nanoparticle distribution with partially fragmented nano-sized TiO$_2$ particles.

deformation is produced, as a result, most of the Al2O3 nanoparticles would be detached from the unreacted TiO2 nanoparticles and dis- persed uniformly in the Al-matrix, which results in the occurrence of Mg2Si phases that subsequently dissolved in the matrix during FSW process [23,47]. Because of this solid-state reaction occurred between TiO2 nanoparticles and Al-matrix, it forms the ultrafine re-precipitated Mg2Si phase (Fig. 7c) along with the formation of some new phases (Fig. 7d, e). Thus, due to this diffusion process, the titanium aluminide (Al3Ti) having a crystallographic relationship with the Al-matrix in planes (112)Al3Ti | (111)Al were formed as shown in Fig. 7f. These re- sults are analogous to the findings of Zhang et al. [11] in which several M23C6 precipitates were formed at the austenitic grain boundaries at higher rotational speed (high heat input), as a result, most of the M23C6 precipitates would be dissolved at all the grain boundaries into the Fe- matrix and new phase of M3C would form during FSW process.

Macro and microstructural features of AA6061-T6 with Al2O3 nanoparticles

Macroscopic features

Fig. 8 shows the macro and microstructural features of AA6061-T6/ Al2O3 friction stir welded samples. Fig. 8a shows the surface mor- phology of the weldment with a well forged and defect-free weld joint having a good surface appearance. Fig. 8b depicts the macrographs for the FSW-Al2O3 sample with no appreciable agglomeration of Al2O3 nanoparticles in advancing and retreating side (RS) due to the occur- rence of vigorous stir action exhibited by local plastically deformed material during FSW process. Macrographs (Fig. 8b) also indicate that the elliptical shape nugget zone was generated which indicates more homogenous intermixing of nanoparticles with the aluminium matrix. Ma et al. [28] have mentioned that the basin shape nugget zone was obtained at lower rotational speed and elliptical shape at a higher ro- tational speed. The obtained results confirmed this phenomenon.

In-depth Al2O3 nanoparticles distribution
In order to understand the in-depth distribution of Al2O3 nano- particles in various zones of FSWed samples, the specimens were cut transversely from the nugget zone and observed for microstructural characteristics using optical microscopy (OM). It was
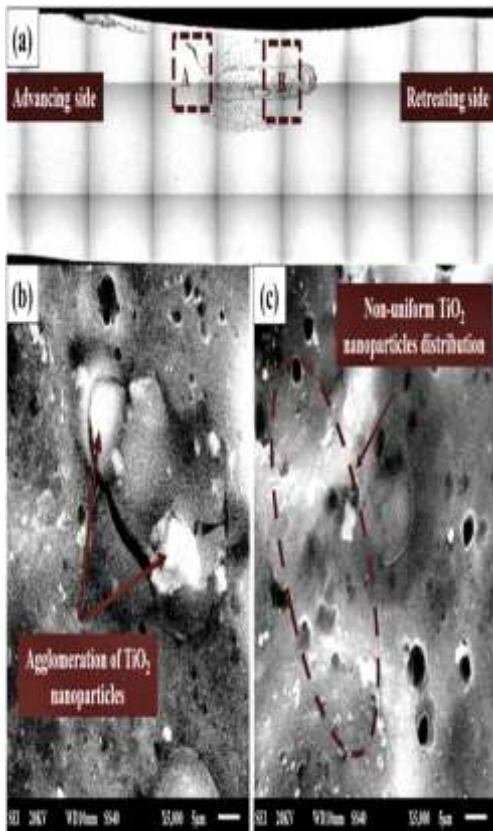

Fig. 6. Transverse section of AA6061-T6- TiO$_2$ processed FSWed sample; (a) Cross-sectional optical micrographs with Region A and Region B, (b)

observed that the great number of Al2O3 nanoparticles would be immersed within the Al- matrix at higher rotating (2000 rpm) and lower traveling (70 mm/min) speed in a single FSW pass. Also, the distribution of Al2O3 nanoparticles for the FSW-Al2O3 sample in the nugget zone is more uniform compared to sample with TiO2 nanoparticles which are attributed to the high density of harder Al2O3 nanoparticles in the Al-matrix. This results in an intense fragmentation process that occurred due to breaking up and symmetric uniform dispersion of small fine particles in the nugget zone centre [10,19,36]. Distribution and size of Al2O3 nanoparticles in the various zone of FSWed-AA6061-T6 joints were explained by using op- tical micrographs as shown in Fig. 8. From Fig. 8, it is clearly depicted that base material has grains elongated in nature having a mean

granular size of 38 µm. The heat-affected zone has a grain size of 39 µm

and experienced only the thermal cycle, as a result, sufficient heat was not produced for nanoparticles to deform plastically (Fig. 8c). There- fore, few agglomerated Al2O3 nanoparticles mainly on AS (Fig. 8b) were formed which leads to strengthening precipitates coarsen and enlargement in the without-precipitate area. It is noteworthy to men- tion that, if the temperature in HAZ is reached above 250 °C then it will exert a pronounced impact on the structure of precipitates [36,48]. Fig. 8d depicts the generation of the fine recrystallized microstructure of grains in the processed zone, which experienced extreme plasticized deformation with uniform Al2O3 nanoparticles distribution, as a result,
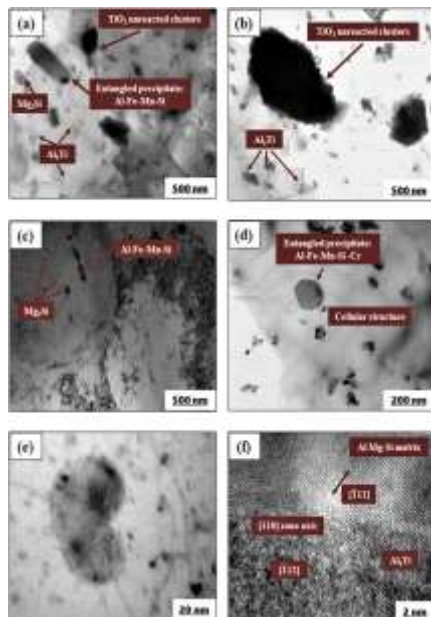
unreacted TiO_2 clusters, (c) ultrafine re-precipitated Mg_2Si phase of Al-Fe-Mn-Si, (d) formation of some new phase of cellular structure, (e) higher magnification in some part of (d), (f) crystallographic relationship between Al_3Ti and Al in planes within the Al-Mg-Si matrix.

the substructures of dislocation are formed inside the grains those are arranged in parallel. The obtained results are in better concurrence with the findings of Mahmoud et al. [19] and Zhang et al. [11]. Also, the generation of fine dynamically recrystallized granular microstructure in the nugget is more attributed to SPD and friction heating occurred during FSW via a phenomenon known as dynamic recrystallization. This phenomenon was distinguished by coalescence and rotation of sub- grain via grain growth and nucleation which leads to the generation of high angle grain boundaries [19,26]. With Al2O3 nanoparticles pre-sence, the processed zone has the granularity of 6 µm which is more

related to the Zener pinning effect which retards the growth of grains in the aluminium metal-matrix. In accordance with this phenomenon, the

addition of nanoparticles affects the distribution of fine nano-sized particulates by providing the Zener-pinning force on high and low angle grain boundaries migration to prevent their motion which counters the force (especially driving) which is responsible for to push these grain boundaries [28,44]. In this study, the limiting grain size was evaluated using the equation proposed by Zener, ($DZ = 4r/3Vf$), where, r and Vf represents the radii and cross-sectional reinforcement fraction (volume) for sample reinforced with Al2O3 nanoparticle and the calculated DZ

was 6.09 µm which is more similar when compared to DZ based on the linear intercept method. From this, it was deduced that with a constant

fraction of volume for nano-sized Al2O3 particles and a decrease in nanoparticles radius, the grain size was significantly reduced. Fig. 8e
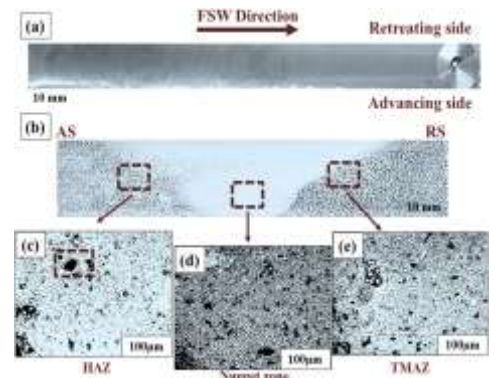

Fig. 7. TEM micrographs of FSW-TiO_2 sample (a) and (b) coarse grain structure with elongated grains having entangled precipitate with

Fig. 8. Macro and micrographs of AA6061-T6- Al_2O_3 processed FSWed sample, (a) Typical surface morphology of sample with Al_2O_3 nanoparticles, (b) (b) Cross- sectional macrographs of FSW- Al_2O_3 weldment, (c) HAZ on AS with few agglomerated Al_2O_3 nanoparticles (Dashed box), (d) NZ with uniform nanoparticles distribution, (e) TMAZ

on RS with more bending grains.

depicts the TMAZ of average grain size 13 μm and experienced both temperature and deformation during FSW because of which it has highly deformed subgrains-structures containing maximum dislocations density those are arranged in a sub-structure and also connected to the precipitates. Fig. 9 shows a transverse section of the AA6061-T6-Al2O3 processed FSWed sample. Fig. 9a clearly represents the more uniform Al2O3 nano-sized particles distribution in the nugget zone which is at- tributed to more intense heat input produced via frictional heating and the pile-up effect exhibited via Al2O3 nanoparticles that helps to pre- vent the further growth of grains accompanied by dynamic re- crystallization throughout FSW process, which lead to more homo- genous distribution of particles with reduction in grain size. Fig. 9b shows the SEM micrograph of heat affected zone and reveals few ag- glomerated Al2O3 nanoparticles that occurred because of the high number of dislocations with coarser precipitates that are formed at the grain boundaries. However, the coarsening of the precipitates in HAZ is governed by the heating cycle or over aging effect occurred in this zone which leads to the decrease in hardness in some regions. Therefore, due to partial fragmentation occurred in the HAZ only a few clusters would break up into small particles and some are agglomerated, later which are distributed uniformly in the nugget zone due to solid-state diffusion occurred via severe plastic deformation during FSW [23,46]. Fig. 9c shows that with the addition of Al2O3 nanoparticles it provides more uniform distribution in the nugget zone, as nano-sized particles act as a site for nucleation and provide hurdles in the migration of grain boundaries and help to prevent the grain growth. Fig. 10 represents the high-resolution TEM micrographs for FSW-Al2O3 samples distinguished with equiaxed fine grains. Fig. 10a, b depicts the presence of Al2O3 nanoparticles in the nugget zone with maximum dislocations density network at the grain interfaces (generally boundaries). This was at- tributed to the SPD process and reactions via diffusion in solid-state which are occurred during the FSW process because of which many

Al2O3 nanoparticles would nucleate and grow at the interface. When the reaction between the Al- Al2O3 particles proceeds further, the ex- cessive deformation is produced, as a result, most of the Al2O3 nano- particles would be dispersed uniformly in the Al- matrix. Whereas Mg2Si phases were subsequently dissolved and few clusters formation in the HAZ (Fig. 10c) during the FSW process would occur [41], which is si- milar to the results reported by Zhang et al. [6]

and Li et al. [7]. Therefore, reinforcement particles play a great role in deformation with respect to the occurrence of dynamic recrystallization followed by grain growth and nucleation [18,42]. Fig. 10d depicts the dispersed Al2O3 nanoparticles (in higher magnification) in the nugget area which is attributed to the availability of reinforcement particulates because of which high strain energy is stored throughout FSW. Therefore, a large amount of localized strain produced around the Al2O3 nanoparticles results in the pace of the rate of nucleation throughout the FSW process.

Micro-hardness measurements

Microhardness was measured 1 mm below the top surface on a transverse section of FSWed AA6061-T6 samples. Measurements were done for specimens (with and without nanoparticles) by taking an equal distance from the weld centreline on each side of the nugget zone as shown in Fig. 11. Microhardness corresponding to different zones of FSW was also evaluated and compared with the as-received parent metal. It can be seen that FSWed samples without nanoparticles addi- tion depict the less microhardness value (51 HV) in the processed zone in comparison to AA6061-T6 which is caused by rising in localized heating via high rotational speed (2000 rpm) and the formation of grain growth which minimizes the hardness value in the weld nugget area. The friction stir welded samples reinforced with both nanoparticles showed higher microhardness value in the nugget zone as compared to the base material. Whereas, the FSW-Al2O3 sample shows the highest
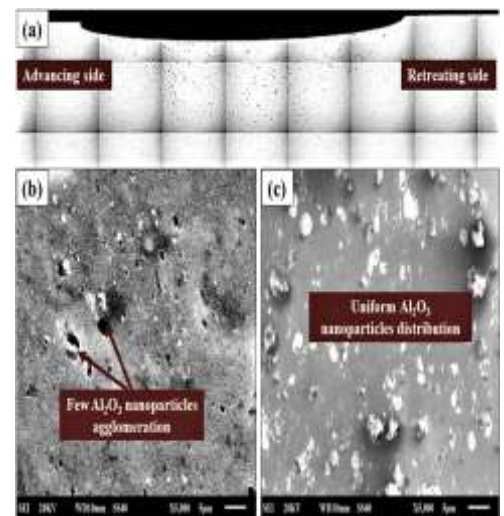

Fig. 9. Transverse section of AA6061-T6- Al$_2$O$_3$ processed FSWed sample; (a) Cross-sectional optical micrographs, (b) SEM micrograph of HAZ on AS show the formation of very few nanoparticles cluster, (c) SEM micrograph of NZ shows the uniform Al$_2$O$_3$ nanoparticle distribution with the fragmented Al$_2$O$_3$ nanoparticles.

microhardness value (89 ± 3 HV) compared to the sample with TiO2 nanoparticles (78 ± 3 HV). This was attributed to the decrease in Al2O3 nanoparticles size that results in increment in microhardness value in accordance with the Hall-Petch effect [30,38]. Also, re-pre- cipitation was possible in the NZ and TMAZ compared to HAZ because of uniformly dispersed fine Al2O3 nanoparticles in the processed zone which provides more nucleation sites for re-precipitation of new grains and precipitates in the aluminium matrix, as a result, the micro-hard- ness value was increased by 73% compared to microhardness of as- received base material. These microhardness results are in better con- currence with the findings of Zhang et al. [6] and Li et al. [7]. In these findings, the highest hardness values were obtained in the stir zone (SZ) with 430 HV which is higher than base material by 170 HV and 225 HV in TMAZ along AS. Similarly, the microhardness variations in the pre- sent study are analogous to the above findings, such that the micro- hardness values in the nugget zone of FSW-Al2O3 and TiO2 sample were

89 ± 3 HV and 78 ± 3 HV HV which is higher than the parent

material microhardness by 43 HV and 32 HV and 63 HV in the TMAZ along AS of the weld. The main strengthening phase exhibits in the FSW-Al2O3 sample is the alignment of Al2O3 nano-sized particles along the weld line and distributed uniformly in the nugget zone than TMAZ which is attributed to the dynamically recrystallized grains occurred in the nugget zone. Also, as the distance from the weld centreline in- creases the grain size in the nugget zone also increases which leads to the fine grain and precipitation strengthening of Al2O3 nanoparticles. Moreover, for the FSW-TiO2 sample, the decrease in the microhardness value apart from the grain refinement (Fig. 5d) is credited to effect which is occurred due to overaging by excessive frictional heating generated in between the shoulder and the tool interface. Therefore, due to intense calefaction, it leads to the fragmentation and amalga- mation of strengthening precipitates which is a more accountable reason for the decrease in microhardness [30,33]. Hence, non-uniform

plasticization caused in the weld nugget of the FSW-TiO2 sample leads to a decrease in the denseness of dislocated sub-grain boundaries that is also responsible for the decrease in the hardenable property, similar results were also reported by Guo et al. [46] and Zhang et al. [6]. Also, because of less hard particles of TiO2 nanoparticles than Al2O3 nano-particles, most of the precipitate will not dissolve in the aluminium matrix during the FSW process, as a result, there was no reappearance of precipitates which leads

to lower hardness in the heat-affected zone and sample fractured from this region during tensile testing.

Mechanical characteristics evaluation

Fig. 12 depicts the result corresponding to the tensile tests done to assess the mechanical properties of FSWed samples (with/without RPs) at 2000 rev·min−1 and 70 mm·min−1 compared with the base material. It has been noted that the mechanical behaviour of FSWed welds merely depends upon (a) grain size, (b) dislocation density, (c) % of agglom- erated particles in the welded zone, and (d) bonding quality [27,36,42]. From Fig. 12a, for the sample without nanoparticles, the tensile strength, yield strength, and % elongation were significantly reduced in comparison to base material which is due to reduction in density of dislocations in the dynamically recrystallized zone, as a result, the fracture of the sample will occur in the nugget zone more towards the AS (Fig. 12b). For the FSW-TiO2 sample, the tensile properties were increased compared to the sample without nanoparticles addition but less than FSW- Al2O3 sample. The decrease in tensile properties was more related to the large nanoparticle cluster formations in the HAZ, as a result, % elongation was significantly reduced which depends on the behaviour of the deformation of aluminium and TiO2 nanoparticles in respect to tensile load. In comparison to TiO2 nanoparticles, aluminium is highly deformable, whereas TiO2 nanoparticles doesn't deform easily and hold back the deformation level of aluminium during the tensile
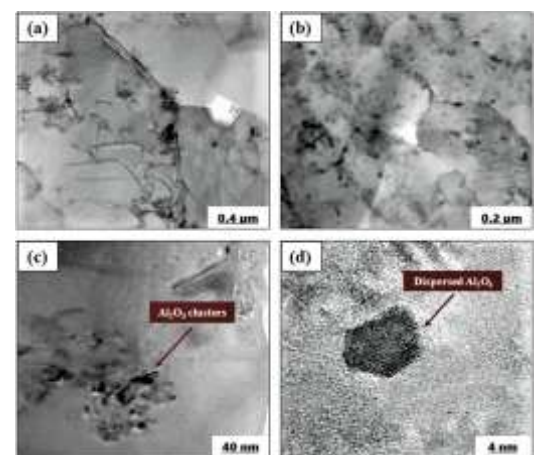

Fig. 10. TEM micrographs of FSW-Al$_2$O$_3$ sample, (a) and (b) fine equiaxed grains with dense dislocation network containing a high density of dislocations, (c) few Al$_2$O$_3$ nanoparticles cluster with dislocations stacked at the grain boundaries in HAZ, (d) uniformly dispersed Al$_2$O$_3$ nanoparticles in the weld nugget zone.
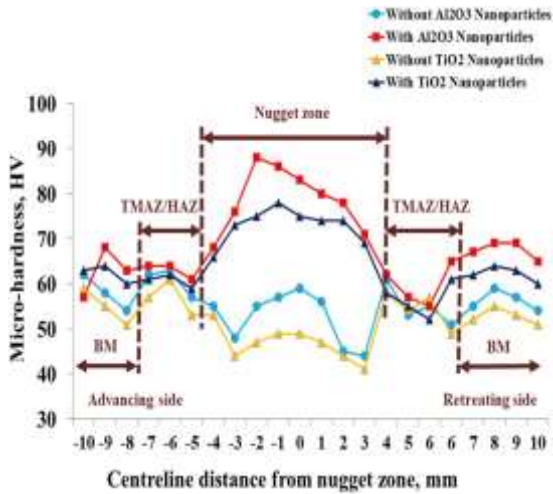
Fig. 11. Microhardness measured transversely for Al_2O_3 and TiO_2 nanoparticles reinforced FSWed AA6061-T6 samples along different zones at equal distance on both sides from the weld centreline towards AS and RS.

and unreinforced samples and compared with AA6061-T6 base material. From Fig. 13, it can be in- ferred that the unreinforced FSWed sample (FSW-W) shows significantly higher volume loss and wear rate (Fig. 13b) in comparison to the base material (Fig. 13a). The higher wear rate is attributed to low microhardness prevailing in the nugget zone due to softening occurred via averaging effect and heating effect at a higher temperature in the
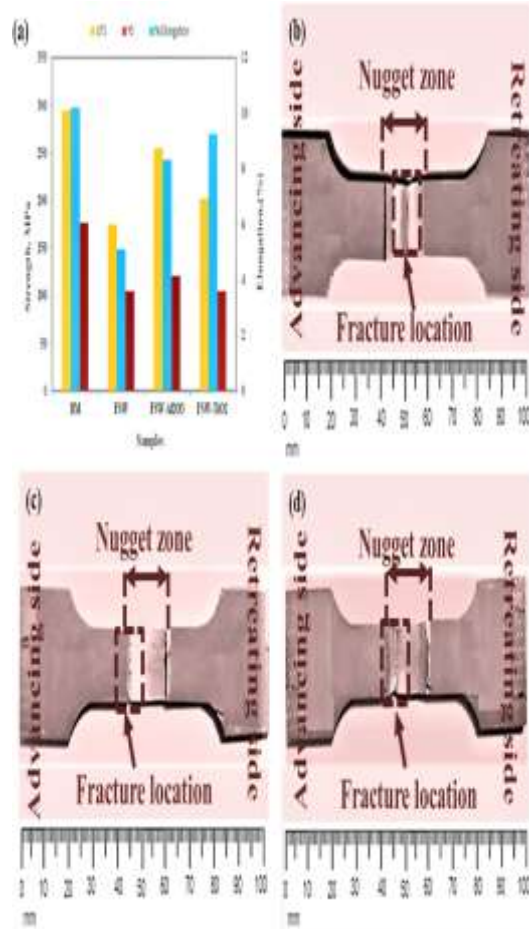

Fig. 12. Extracted values of tensile properties for Al_2O_3 and TiO_2 nanoparticles reinforced and unreinforced samples, (b-d) Fracture locations of the FSWed samples after tensile loading.

test which leads to decrease in ductility, as a result, the fracture of the sample will occur at TMAZ on AS is shown in Fig. 12c. Whereas for the FSW-Al2O3 sample, the tensile properties, namely, tensile strength, yield strength and % elongation was significantly increased as com- pared to sample without nanoparticles and FSW-TiO2 samples. This was due to the existence of uniformly dispersed higher density of harder

Al2O3 nanoparticles in the welded area at 2000 r·min−1 and 70 mm·min−1 in Al-matrix. Also, grain size drop results in an increase of strengthening at the grain boundaries via (a) high dislocation density due to thermal mismatch index, (b) restrictions occurred in the path of grain boundaries which provides more nucleation sites and prevents the grain growth at the grain boundaries [42,49] as these outcomes are in better concurrence with the findings of Zhang et al. [11] and Li et al. [7]. Due to these reasons, the fragmentation process is more intense; as a result, most of the Al2O3 nanoparticles would break up into small fine particles and uniformly distributed in the nugget zone. Hence, more uniform nanoparticles distribution and symmetric flow would occur in the nugget zone centre. Therefore, re-precipitation of strengthening precipitates leads to more coarsening and dissolution of precipitates which helps in retaining the maximum tensile strength and yield strength with an appreciable enhancement in elongation, as a result, the fracture of the sample will occur in HAZ more towards the base metal on AS as depicted in Fig. 12d.

Wear measurements

Fig. 13 depicts the results pertaining to the wear test conducted for Al2O3 and TiO2 nanoparticles reinforced

weldment [19]. In accordance with Archard's law of wear [50], the loss in volume is inverse to the microhardness of the produced weld via FSW, as metal removal rate decreases during sliding wear. Whereas, welds reinforced with Al2O3 and TiO2 nanoparticles showed remarkable enhancement in the wear resistance due to lower loss in volume and rate of wear compared to the unreinforced joint (Fig. 13c, d). Increment in wear resistance of reinforced FSWed samples is ascribed to higher microhardness value due to microstructure evolutions and grain re- finement during the FSW process. In accordance with Fig. 13, the im- provement in the frictional coefficient of unreinforced and reinforced samples was observed in comparison to the base material. This en- hancement

was attributed to the adhesion caused by the reinforced particles which lead to abrasion on the surface and results in the for- mation of ups and downs path during wear [32,40,51]. From Fig. 13c, it can be inferred that FSW-Al2O3 samples experienced low frictional coefficient and higher wear resistance in comparison to the un-

reinforced sample. This was attributed to fine small grains size (6 μm)

in the nugget zone and large distribution of microhardness (89 ± 3 HV) which leads to a reduction in coefficient of friction on account of the reason that, these fine equiaxed Al2O3 nano-sized par- ticles were uniformly dispersed in the aluminium-parent matrix (Fig. 8d), these results are analogous to Prakash et al. [26] findings. Consequently, a low coefficient of friction for sample reinforced with Al2O3 nanoparticles implies that the wear mechanism is mainly abra- sive due to the harder surface which puts the scratches over the softer surface [44,48]. Whereas, for the FSW-TiO2 sample, it experienced a higher frictional coefficient and lower wear resistance compared to sample reinforced with Al2O3 nanoparticles and unreinforced sample.

This was attributed to the agglomeration of TiO2 nanoparticles in the HAZ on the advancing side, as a result, poor adhesion between nano- sized TiO2 particles and the aluminium metal matrix would occur. Therefore, separation of coated overlay surface instead of erosion would occur, as a result, large weight loss due to localized welding of worn debris to the sample surface could happen.

Conclusions

When combining AA6061-T6 butt joints reinforced with nanoparticles at the abutting edges, friction stir welding is a better technique to use. As a result of decreased relative velocity, temperature, and heat (friction) between the tool and the non-uniformly deformed plasticized material, the distribution of nanoparticles in the sample reinforced with Al2O3 nanoparticles is more homogeneous and free of surface defects than in the TiO2 nanoparticles reinforced sample, which exhibits agglomeration of nanoparticles in HAZ on AS. While partial fragmentation occurred in the case of the FSW-TiO2 sample due to the dynamic action caused by the rotational speed and vortex ring with the forward movement of the tool, complete fragmentation of intermetallic compounds and Al2O3 reinforced nanoparticles occurred in the FSW-Al2O3 sample, which is attributed to the action of higher localized heat input at high rotating tool speed (2000 rpm) and moderate welding speed (70 mm/min).

Through concurrent reactions of severe plastic formation and friction heating throughout the FSW process, Al2O3 nanoparticle-reinforced samples exhibit a finely recrystallized structure of grains with a mean granularity of 6 μm, according to microstructural studies. The samples supplemented with TiO2 nanoparticles have an average grain size of 8 μm, and there are few particle clusters or agglomerations in the HAZ. This is because the heating and overaging impact of the FSW process at high temperature coarsens the precipitates. In the processed nugget zone, the FSW-Al2O3 samples display a higher microhardness distribution of 89 ± 3 HV. This is attributed to uniform Al2O3 nanoparticles within the Al-matrix and is consistent with the phenomenon known as the Hall-Petch relationship (fine grains morphology in the weld zone). In contrast, the FSW-TiO2 samples exhibit a lower microhardness of 78 ± 3 HV, which is caused by intermittent plasticization in the weld nugget area. This phenomenon results in a decrease in the density of dislocated boundaries containing sub-grains, which in turn causes strengthening precipitates to become coarse and dissolve in the nugget zone.

References

[1] R.W. Hertzberg, Deformation and Fracture Mechanics of Engineering Materials, 4th ed., Wiley, 1996, p. 747.

[2] J.G. Kaufman, Introduction to Aluminium Alloys and Tempers, ASM Int, 2000, p. 242.

[3] M.J. Starink, A. Deschamps, S.C. Wang, The strength of friction stir welded and friction stir processed aluminium alloys, Scripta Mater 58 (5) (2008) 377–382.

[4] R.S. Mishra, Z.Y. Ma, Friction stir welding and processing, Mater. Sci. Eng. R 50 (2005) 1–78.

[5] J.F. Daniel, D.M. Justin, R.Z. Michael, E.P. Frank, Solid-state infiltration of 6061-T6 aluminium alloy into carbon fibers via friction stir welding, J. Manuf. Sci. Eng. 139 (11) (2017) 111014–111014–111019.

[6] C. Zhang, L. Cui, Y. Liu, C. Liu, H. Li, Microstructures and mechanical properties of friction stir welds on 9% Cr reduced activation ferritic/martensitic steel, J. Mater. Sci. Technol. 34 (5) (2018) 756–766.

[7] Y. Li, Y. Liu, C. Liu, C. Li, Z. Ma, Y. Huang, Z. Wang, W. Li, Microstructure evolution and mechanical properties of linear friction

welded S31042 heat-resistant steel, J. Mater. Sci. Technol. 34 (4) (2018) 653–659.

[8] P. Praveen, P.K.D.V. Yarlagadda, Meeting challenges in welding of aluminium al- loys through pulse gas metal arc welding, J. Mater. Process. Technol. 164–165 (2005) 1106–1112.

[9] B. Arivazhagan, G. Srinivasan, S.K. Albert, A.K. Bhaduri, A study on influence of heat input variation on microstructure of reduced activation ferritic martensitic steel weld metal produced by GTAW process, Fusion Engineering and Design 86 (2–3) (2011) 192–197.

[10] P. Cavaliere, A.D. Santis, F. Panella, A. Squillace, Effect of welding parameters on mechanical and microstructural properties of dissimilar AA6082–AA2024 joints produced by friction stir welding, Mater. Des. (2009) 609–616.

[11] C. Zhang, L. Cui, D. Wang, Y. Liu, C. Liu, H. Li, The heterogeneous microstructure of heat affect zone and its effect on creep resistance for friction stir joints on 9Cr–1.5 W heat resistant steel, Scr. Mater. 158 (2019) 6–10.

[12] M. Aissani, S. Gachi, F. Boubenider, Y. Benkedda, Design and optimization of friction stir welding tool, Mater. Manuf. Process. 25 (11) (2010) 1199–1205.

[13] A. Lauro, Friction stir welding of titanium alloys, Weld. Int. 26 (1) (2012) 8–21.

[14] A. Pradeep, S. Muthukumaran, P. Dhanush, Sub-shoulder formation during friction stir welding of steel using tungsten alloy tool, Sci. Technol. Weld. Join. 18 (8) (2013) 671–679.

[15] W.B. Lee, S.B. Jung, The joint properties of copper by friction stir welding, Mater. Lett. 58 (6) (2004) 1041–1046.

[16] S. Rouhi, A. Mostafapour, M. Ashjari, Effects of welding environment on micro- structure and mechanical properties of friction stir welded AZ91C magnesium alloy joints, Sci. Technol. Weld. Join. 21 (1) (2016) 25–31.

[17] M. Saeidi, M. Barmouz, M. Kazem, B. Givic, Investigation on AA5083/ AA7075+Al_2O_3 joint fabricated by friction stir welding: characterizing micro- structure, corrosion and toughness behaviour, Mater. Res. 18 (6) (2015) 1156–1162.

[18] M.A. Pasha, P.R. Reddy, P. Laxminarayana, I.A. Khan, SiC and Al_2O_3 reinforced friction stir welded joint of aluminium alloy 6061, International Journal of Precision Engineering and Manufacturing-Green

[19] E.R.I. Mahmoud, M. Takahashi, T. Shibayanagi, K. Ikeuchi, Effect of the friction stir processing tool probe on the fabrication of SiC particle reinforced composite on the aluminium surface, Sci. Technol. Weld. Join. 14 (2009) 413–425.

[20] A.A.K. Suban, M. Perumal, A. Ayyanar, A.V. Subbiah, Microstructural analysis of B_4C and SiC reinforced Al alloy metal matrix composite joints, Int. J. Adv. Manuf. Technol. 93 (1–4) (2017) 515–525.

[21] D. Jayabalakrishnan, M. Balasubramanian, Eccentric-weave friction stir welding between Cu and AA 6061-T6 with reinforced graphene nanoparticles, Mater Manuf Proces 33 (3) (2018) 333–342.

[22] F. Cioffi, R.F. Serrano, D. Gesto, P.R. Rodriguez, G.G. Doncel, D. Verdera, Friction stir welding of thick plates of aluminium alloy matrix composite with a high volume fraction of ceramic reinforcement, Compos. A: Appl. Sci. Manuf. 54 (2013) 117–123.

[23] M. Dixit, J.W. Newkirk, R.S. Mishra, Properties of friction stir-processed Al1100-NiTi composite, Scr. Mater. 56 (2007) 541–544.

[24] J. Gandra, R. Miranda, P. Vilac, A. Velhinho, P.T.J. Producing, Functionally graded materials by friction stir processing, J. Mater. Process. Technol. 211 (2011) 1659–1668.

[25] C.M.A. Fernández, R.A. Rey, M.J.C. Ortega, D. Verdera, C.L. Vidal, Friction stir processing strategies to develop a surface composite layer on AA6061-T6, Mater. Manuf. Process. 33 (10) (2018) 1–8.

[26] T. Prakash, S. Sivasankaran, P. Sasikumar, Mechanical and tribological behaviour of friction-stir-processed Al 6061 aluminium sheet metal reinforced with Al_2O_3/0.5Gr Al_2O_3/0.5Gr hybrid surface nanocomposite, Int. J. Adv. Manuf. Technol. 80 (9–12) (2015) 1919–1926.

[27] A. Sharma, V.M. Sharma, S. Mewar, S.K. Pal, J. Paul, Friction stir processing of Al6061-SiC -graphite hybrid surface composites, Mater. Manuf. Process. 33 (7) (2018) 795–804.

[28] Z.Y. Ma, R.S. Mishra, M.W. Mahoney, Friction stir processing for microstructural modification of an aluminium casting, in:

K.V. Jata, M.W. Mahoney, R.S. Mishra, S.L. Semiatin, T. Lienert (Eds.), Friction Stir Welding and Processing II, TMS, 2003, pp. 21–30.

[29] P. Karthikeyan, K. Mahadevan, Investigation on the effects of SiC particle addition in the weld zone during friction stir welding of Al 6351 alloy, Int. J. Adv. Manuf. Technol. 80 (9–12) (2015) 1919–1926.

[30] J. Guo, B.Y. Lee, Z. Du, B. Guijun, J.M. Tan, W. Jun, Effect of nano-particle addition on grain structure evolution of friction stir processed Al 6061 during post-weld annealing, Arab. J. Sci. Eng. 40 (2) (2015) 559–569.

[31] M. Barmouz, G.M.K. Besharati, J. Seyfi, On the role of processing parameters in producing Cu/SiC metal matrix composites via friction stir processing: investigating microstructure, microhardness, wear, and tensile behaviour, Mater Character 62 (2011) 108–117.

[32] M. Bahrami, F.N. Mohsen, K.B.G. Mohammad, Microstructural and mechanical behaviours of nano-SiC-reinforced AA7075-O FSW joints prepared through two passes, Mater. Sci. Eng. A A626 (2015) 220–228.

[33] R. Thirumalai, K.J.S. Senthil, Intelligent selection of optimum machining para-meters in turning of Inconel 718, Int J Adv Eng Technol 2 (4) (2011) 167–173.

[34] R.A. Adalarasana, S. Sundaram, Study of friction welding characteristics of Al/SiC composite and application of grey-based TOPSIS, J. Chin. Inst. Eng. (2016) 1–9.

[35] Y.F. Sun, H. Fujii, The effect of SiC particles on the microstructure and mechanical properties of friction stir welded pure copper joints, Mater. Sci. Eng. A 528 (16) (2011) 5470–5547.

[36] T. Singh, S.K. Tiwari, D.K. Shukla, Friction stir welding of AA6061-T6: the effects of Al2O3 nano-particles addition, Results in Materials 1 (2019) 100005.

[37] J. He, Z. Ling, H. Li, Effect of tool rotational speed on residual stress, micro- structure, and tensile properties of friction stir welded 6061-T6 aluminium alloy thick plate, Int. J. Adv. Manuf. Technol. 84 (9–12) (2016) 1953–1961.

[38] F.J. Liu, L. Fu, H.Y. Chen, Effect of high rotational speed on temperature distribu-tion, microstructure evolution, and mechanical properties of friction stir welded 6061-T6 thin plate joints, Int. J. Adv. Manuf. Technol. 96 (5–8) (2018) 1823–1833.

[39] I. Shigematsu, Y.J. Kwon, K. Suzuki, T. Imai, Joining of 5083 and 6061 aluminium alloys by friction stir welding, J. Mater. Sci. Lett. 22 (5) (2003) 353–356.

[40] J.K. Doley, S.D. Kore, A study on friction stir welding of dissimilar thin sheets of aluminium alloys AA 5052–AA 6061, J. Manuf. Sci. Eng. 138 (11) (2016) 114502–114502–114506.

[41] H. Fujii, L. Cui, K. Nakata, K. Nogi, Mechanical properties of friction stir welded carbon steel joints -friction stir welding with and without transformation, Welding in the World 52 (9–10) (2008) 75–81.

[42] D.F. Scialpi, P. Cuomo, P.D. Summa, Micro-friction stir welding of 2024–6082 aluminium alloys, Weld. Int. 21 (1) (2008) 16–22.

[43] A. Ajri, Y.C. Shin, Investigation on the effects of process parameters on defect formation in friction stir welded samples via predictive numerical modelling and experiments, J. Manuf. Sci. Eng. 139 (11) (2017) 111009–111009–111010.

[44] W. Woo, L. Balogh, T. Ungár, H. Choo, Z. Feng, Grain structure and dislocation density measurements in a friction-stir welded aluminium alloy using X-ray peak profile analysis, Mater. Sci. Eng. 498 (1–2) (2008) 308–313.

[45] J.M. Root, D.P. Field, T.W. Nelson, Crystallographic texture in the friction-stir-welded metal matrix composite Al6061 with 10 Vol Pct Al_2O_3, Metall. Mater. Trans. A 40 (9) (2009) 2109–2114.

[46] J. Guo, P. Gougeon, X.G. Chen, Microstructure evolution and mechanical properties of dissimilar friction stir welded joints between AA1100-B_4C MMC and AA6063 alloy, Mater. Sci. Eng. A 553 (2012) 149–156.

[47] F.J. Humphreys, M. Hatherly, Chapter 13-hot deformation and dynamic restoration, Recrystallization and Related Annealing Phenomena, Elsevier Ltd, 2004, pp. 415–450.

[48] F.J. Humphreys, M. Hatherly, Chapter 11-grain growth following recrystallization, Recrystallization and Related Annealing Phenomena, Elsevier Ltd, 2004, pp.

333–378.

[49] C.J. Tweed, B. Ralph, N. Hansen, The pinning by particles of low and high angle grain boundaries during grain growth, Acta Metall. 32 (9) (1984) 1407–1414.

[50] G. Minak, L. Ceschini, I. Boromei, M. Pontec, Fatigue properties of friction stir welded particulate reinforced aluminium matrix composites, Int J of Fatigue 32 (2010) 218–226.

[51] J. Martin, Micromechanisms in Particle Hardened Alloy, Cambridge University Press, Cambridge, 1980.